ELSEVIER

Ceramics International 30 (2004) 931–938

CERAMICS INTERNATIONAL

www.elsevier.com/locate/ceramint

Preparation and characterisation of aluminium nitride–silicon carbide composites

Inger-Lise Tangen [a], Yingda Yu [b], Tor Grande [a], Tommy Mokkelbost [a], Ragnvald Høier [b], Mari-Ann Einarsrud [a,*]

[a] *Department of Materials Technology, Norwegian University of Science and Technology, 7491 Trondheim, Norway*
[b] *Department of Physics, Norwegian University of Science and Technology, 7491 Trondheim, Norway*

Received 1 September 2003; received in revised form 16 September 2003; accepted 11 November 2003

Available online 9 April 2004

Abstract

Aluminium nitride–silicon carbide (AlN–SiC) composites were prepared to increase the fracture toughness of AlN-based ceramics. The composites (0–30 vol.% SiC) were made by pressureless sintering at 1870 °C, using Al_2O_3–Y_2O_3 (2 wt.%) as sintering additive. The solubility of SiC in AlN was determined to be between 10 and 15 vol.% at 1870 °C. Particulate AlN composites were formed for >10 vol.% SiC and the SiC grains acted as grain boundary pinning centres during sintering. Vickers hardness and Young's modulus increased monotonically when adding SiC, 65% for 30 vol.% SiC and 13% for 20 vol.% SiC, respectively. Both bending strength and fracture toughness increased ~22% when 20 vol.% SiC was added. The toughening of the composites is mainly caused by residual strain due to thermal expansion or elastic modulus mismatch between SiC grains and the AlN–SiC matrix. Elongated α-SiC grains were observed for >15-vol.% SiC materials, which increased the toughening of the materials. The fracture toughness was also calculated using various models based on Vickers indentation, and most models underestimated the fracture toughness compared to the single edge notched beam (SENB) method.

Keywords: B. Composites; B. Microstructure-final; C. Toughness and toughening; D. SiC; AlN

1. Introduction

Aluminium nitride is a ceramic material with high thermal conductivity combined with high electrical resistance, low thermal expansion, high corrosion resistance and low density. Due to the rare combination of properties, AlN is attractive for refractory applications such as metal handling, in semiconductor devices and as heat sinks, electronic substrates, grinding media, seals, filler materials, etc. Enhanced mechanical performance, i.e. improved fracture toughness of AlN will allow new uses in structural applications. Witek et al. [1] reported a fracture toughness of $3.6 \pm 0.6\,\mathrm{MPa\,m^{1/2}}$ for fully dense hot-pressed AlN (biaxial testing of disk [2]), Huang and Jih [3] and Hagen et al. [4] reported 3.5–4 $\mathrm{MPa\,m^{1/2}}$ for hot-pressed AlN without sintering additives and $3.6 \pm 0.2\,\mathrm{MPa\,m^{1/2}}$ for pressureless sintered AlN with CaO–Al_2O_3 sintering additives, respectively, using the single edge notched beam (SENB) method. Mariano et al. [5] reported $2.9 \pm 0.7\,\mathrm{MPa\,m^{1/2}}$ for hot-pressed AlN, measured by the single edge pre-cracked beam (SEPB) method. Lower fracture toughness values down to $2.0\,\mathrm{MPa\,m^{1/2}}$ have also been reported [6–13].

To increase the fracture toughness of AlN, two different strategies have been used: optimisation of the sintering additives and particle reinforcement. Particle-reinforced AlN ceramics have been made with various non-metallic secondary particles, e.g. TiN [8,9,14–17], BN [9,18,19] and both TiN and BN [9].

The by far most used secondary phase in particle reinforced AlN is silicon carbide (SiC), although most studies have been performed on SiC-rich materials. AlN–SiC materials are mainly prepared by hot pressing [3,5,11,12,20–27], but also pressureless sintering [10,28–30] is reported. A tentative phase diagram for AlN–SiC is presented by Zangvil and Ruh [31] showing a large composition range of solid solution above 1950 °C. Particulate AlN composites can be prepared either directly or by spinodal decomposition

* Corresponding author. Tel.: +47-73-59-40-02; fax: +47-73-59-08-60.
E-mail address: Mari-Ann.Einarsrud@material.ntnu.no (M.-A. Einarsrud).

0272-8842/$30.00
doi:10.1016/j.ceramint.2003.11.006

of AlN–SiC solid solution by annealing in the two-phase region.

The hardness of AlN–SiC composites increases strongly with increasing SiC content, both in particulate composites [3,10,12,27–29] and in solid solution materials [11,24,26]. The strength of the AlN–SiC composites show no unambiguous trends, neither for particulate composite [3,5,10,12,21,22] nor for solid solution AlN–SiC [11,20,24,26]. The variation in reported strength is large, due to the strong dependence of fracture strength on microstructure and measuring methods. Young's modulus is reported to increase with increasing SiC content in AlN–SiC solid solution materials [11,25].

The fracture toughness of particulate AlN–SiC materials generally increases with increasing SiC content [3,5,10,12,27,28]. Li and Watanabe [10] report a fracture toughness increase from 2.01 to 3.83 MPa $m^{1/2}$ when forming 30-vol.% SiC materials, in contrast to an increase from ∼3.5 to ∼3.7 MPa $m^{1/2}$ reported by Lee and Wei [28], both for liquid phase sintered materials. The fracture toughness in particulate composites is significantly higher compared to solid solution materials with the same phase content [3,28,29]. The toughening mechanism of SiC particles is not well established. Both crack deflection around SiC particles [3,28] and transgranular fractures of the SiC grains [3,29] have been reported. Huang and Jih [3] suggested that formation of a solid solution layer between SiC and AlN grains lowers the tendency for crack deflection. Residual strain due to thermal expansion and elastic modulus mismatch is also proposed to cause the reinforcing effect [3,29].

Even though a large number of studies have been performed in the AlN–SiC system, the emphasis has been on SiC-rich materials and little knowledge about mechanical properties is presented on AlN-based composites. The major goal of this work was to study the toughening effect of SiC in pressureless sintered AlN–SiC particulate composites. To achieve knowledge of the toughening mechanism, low SiC containing composites were prepared and carefully characterised. The phase relations and microstructure and their influence on the mechanical properties were investigated and the solid solubility limit for SiC in AlN at 1870 °C was determined. A comparison study was performed between fracture toughness measured by the SENB method and calculated by various different models based on a Vickers indentation method.

2. Experimental

AlN–SiC composites were prepared from AlN powder (Tokuyama Soda, Grade F, containing 0.6 wt.% oxygen on the grain surface) and SiC powder (Norton, F1200, α-phase). SiC powder in the range from 1 to 3 μm was prepared by sedimentation. Al_2O_3 (Alcoa, A 16 SG) (1.6–1.7 wt.%) and Y_2O_3 (H.C. Starck, quality Finest) (0.9 wt.%) were added as sintering aids. The SiC content in the composites varied between 0 and 30 vol.%.

The powders were mixed in 100% ethanol by ball milling for four hours using alumina balls. Soft agglomerates (<500 μm) were formed by sieving before preparation of bars for mechanical testing. The powder was either uniaxially pressed into pellets (ϕ 15 mm) at 230 MPa or into bars, which were first uniaxially pressed at 15 MPa and then isostatically pressed at 200 MPa. Ethyl cellulose (Sigma) (2 wt.%) was used as binder. The green density of both bars and pellets was approximately 56%.

The materials were sintered in N_2-atmosphere in a graphite resistance furnace described by Herstad and Motzfeldt [32]. The AlN–SiC pellets were sintered in a molybdenum (Mo) crucible with a lid and the AlN–SiC bars in a SiC-crucible with lid and a coarse SiC powder bed. For the bars sintered in SiC crucibles the heating and cooling rate was 300 K/h. The heating and cooling rate for the pellets was 2000 K/h below 1650 °C and 1000 K/h above 1650 °C. All the materials were kept at the maximum temperature of 1870 °C for 6 h. Details for the sintering of the pure AlN bars are described elsewhere [14]. The density was determined by Archimedes' method using isopropanol. The theoretical density was calculated from the law of mixtures and was not corrected for weight loss during sintering.

The microstructure of the materials was studied by scanning electron microscopy (SEM) (Hitachi S3500N), optical microscopy (Reickert MeF3 A) and transmission electron microscopy (TEM) (Philips CM30) equipped with energy dispersive spectroscope (EDS) (Edax International). TEM specimens were prepared from the interior of the samples as described elsewhere [14]. Phase composition was studied by powder X-ray diffraction (XRD) using a Siemens D5005 X-ray diffractometer. The ceramics were ground to powder prior to XRD measurements. Silicon powder (10–15 wt.%) was added as an internal standard for *d*-value calibration. Lattice parameters were calculated using the programs Win-Index and Win-Metric from Bruker axs. The grain size of the sintered materials was measured on polished surfaces thermally etched at 1600 °C for 0.2 h. About 300–500 AlN grains were measured using the linear intercept method.

Bending strength and Young's modulus (*E*-modulus) of the SiC containing materials were measured using a four point bending test. Bars were machined to MIL SPEC 1942 and dimensions 4 mm × 3 mm × 45 mm and all the edges were chamfered. The testing was performed in a 4-point flexure 40 mm × 20 mm span set-up in an electromechanical test machine (Cormet) with a 20 kN uniaxial actuator (Cormet digital control) and a 2 kN HBM load cell was used for data recording. The load signal was recorded by a FLUKE logging system. High temperature α-SiC push-rods (MTS 602.81) were attached to water-cooled grips. The sample was mounted in a high-temperature bend fixture (MTS 642.85), constructed of α-SiC and designed to comply with ASTM Standard C1211-92 for high-temperature bend testing. The fixture was fully articulating to minimise

high contact stresses. The rollers were designed to both roll and pivot to ensure a line contact on the specimen. The calculation of Young's modulus was based on an equation of deflection described by Sass et al. [33]. The deflection was measured during bending strength tests using an MTS bend bar extensometer (632.70-03). The deflection of the sample was measured using three α-SiC rods extended from the extensometer up to the test specimen. The two outer rods were spaced to correspond with the location of the two upper rollers, and the deflection of the centre rod with respect to the outer rods was measured. All measurements were performed in displacement control at a crosshead rate of 8 μm/s. A total of 8–10 specimens were tested for each composition. The fracture surfaces were studied by SEM to reveal the fracture origins. The mechanical testing of the pure AlN materials is described elsewhere [14].

The fracture toughness of the SiC containing materials was determined using the single edge notched beam method (SENB). The testing was performed in the same mechanical testing rig as described above. The testing bar dimensions used were 3 mm × 4 mm × 45 mm. The depth of the notches was 1.2 mm and the width about 0.2 mm. Fracture toughness was calculated using ISO 15732 [34]. A total of 3–4 specimens were tested for each composition. The fracture toughness was also determined for all the specimens in flowing N_2-atmosphere (max 230 ppm O_2) at 800 °C (both pure AlN and AlN–SiC composites). The mechanical testing rig was fitted with a split single phase Kanthal A heating element (SIGMATEST Materialprüftechnik GmbH) and Ni radiation shields and was mounted inside a water-cooled vacuum chamber connected to a rotary pump and a gas supply system.

Hardness was measured using the Vickers indentation method on polished surfaces. Fracture toughness was also determined from Vickers indents at high load to compare to the values obtained by the SENB method. An Akashi AVK-C1 Hardness Tester was used for the indentation and a Reickert MeF3 An optical microscope with a Sony DXC-930P Colour Video Camera and the program NIH Image for measuring of indents and crack lengths. Vickers hardness, H_V, was calculated using the equation reported by Anstis et al. [35]. Fracture toughness, K_{IC}, was calculated from various different equations presented by Ponton and Rawlings [36]. Vickers hardness was calculated from 2.9 N indents and fracture toughness from 49.05 N indents. Ten indents were made for each composition and load.

3. Results

Relative density and weight loss during firing of AlN and AlN–SiC composites are plotted in Fig. 1. AlN and AlN–SiC composites with <25 vol.% SiC obtained a high density (>99% of theoretical density). When the SiC content was further increased the density decreased to 93 ± 2%. The different sintering conditions for bars and pellets gave no

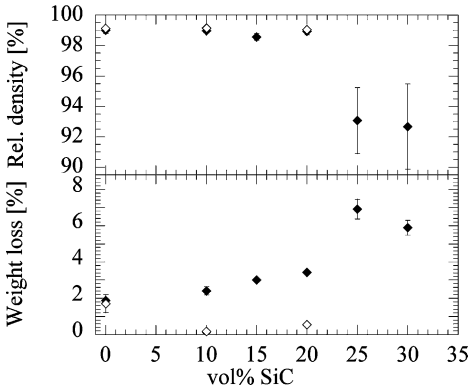

Fig. 1. Relative density and weight loss during firing of AlN and AlN–SiC composites. The filled diamonds represent pellets sintered in Mo-crucibles and the open diamonds are bars sintered in SiC-crucibles or graphite crucibles lined with Mo-foil. The error bars represent the standard deviation.

variations in relative density. The weight loss during sintering increased with increasing SiC content. The weight loss was found to be considerably lower for bars sintered in the SiC crucibles, because the SiC crucible assembly was tighter than the Mo crucibles/linings used for pellets and pure AlN bars.

AlN, various α-SiC polytypes and yttrium aluminium garnet (YAG), $Al_5Y_3O_{12}$, or yttrium aluminium perovskite (YAP) $AlYO_3$, were identified by XRD in the AlN and AlN–SiC materials. YAG or YAP are formed from the AlN containing Al_2O_3–Y_2O_3 liquid phase during cooling, dependent on the crystallisation path. According to the quasi-binary Al_2O_3–Y_2O_3 phase diagram [37], either YAG or YAP can be stable. Studies in the ternary AlN–Al_2O_3–Y_2O_3 system show nitrogen stabilisation of the YAP phase [38]. Traces of SiAlON were also observed for materials containing >10 vol.% SiC. SiC was not identified in the 10-vol.% SiC material, but a shift in the diffraction peaks of AlN was observed. The AlN lattice parameters (*a* and *c*) are plotted in Fig. 2 together with the lattice parameters for the AlN–SiC solid solution assum-

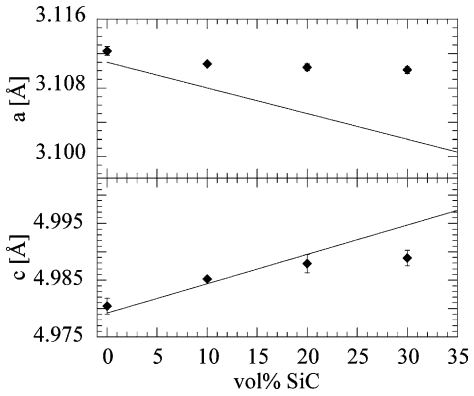

Fig. 2. Lattice parameters of AlN in AlN–SiC composites vs. SiC content. The lines are the linear mixing between lattice parameters for pure AlN and SiC (Vegard's law) [39,40].

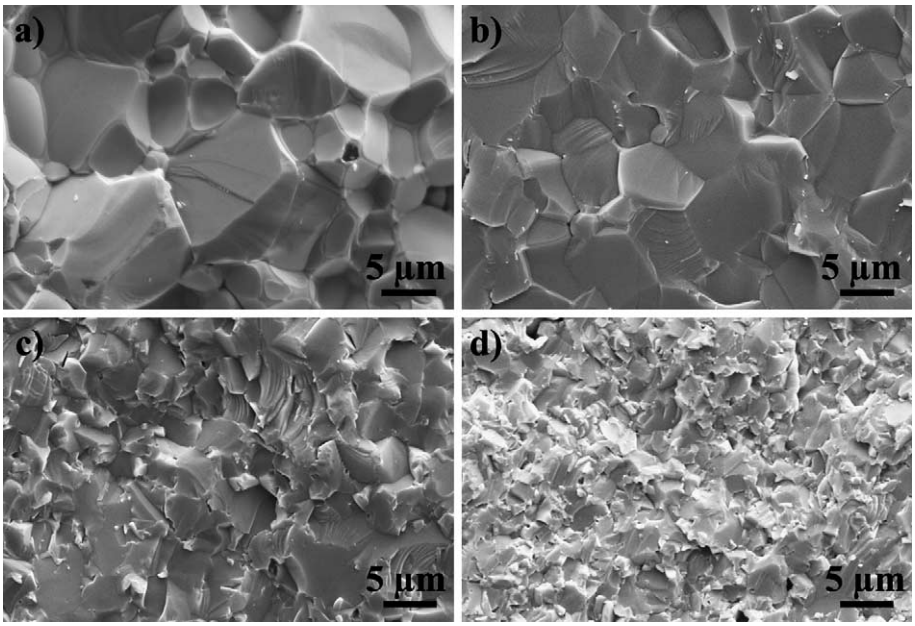

Fig. 3. SEM images of fracture surfaces of AlN and AlN–SiC composites: (a) AlN, (b) 10 vol.% SiC, (c) 20 vol.% SiC and (d) 30 vol.% SiC.

ing Vegard's law [39,40]. Up to 10 vol.% SiC, the *a* and *c* parameters are consistent with the lattice parameter of the solid solution, but above 10 vol.% SiC both cell parameters are independent of the SiC content.

SEM images showing fracture surfaces of AlN and AlN–SiC composites containing 10, 20 and 30 vol.% SiC are given in Fig. 3. No contrast between AlN and SiC grains is observed due to similar average atomic number. The materials show mainly transgranular fracture mode, except the pure AlN where the fraction of intergranular fractures is high. The grain size of AlN decreases with SiC content. This decrease is also demonstrated in Fig. 4 where the grain size of AlN versus SiC content is plotted. The grain size of a small area without SiC-grains (due to inhomogeneous distribution of SiC) in the 25 vol.% SiC-material is included in Fig. 4 and this area has about the same grain size as the 10-vol.% SiC material. From Figs. 3 and 4 it is clear that SiC grains significantly inhibits grain growth of AlN in AlN–SiC composites.

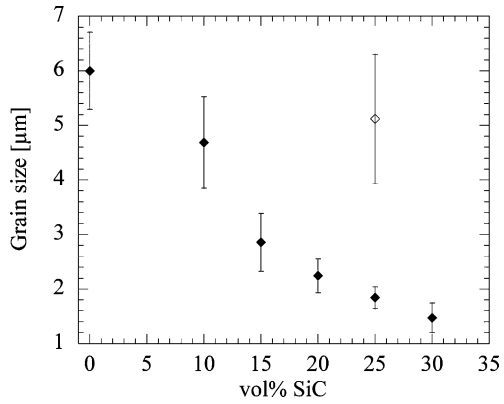

Fig. 4. Grain size of AlN in AlN–SiC composites. The open diamond represents the grain size in an area of the 25-vol.% SiC sample without SiC grains. The error bars represent the variation in grain size (standard deviation).

Low magnification TEM images of the composites are given in Fig. 5 confirming the decrease in grain size with increasing SiC content. The SiC grains are seen as smaller medium dark contrast grains. No SiC grains were observed in the 10-vol.% SiC material. The dark contrast Y_2O_3–Al_2O_3 sintering additive is located at triple junctions and grain boundaries. From EDS analysis, solid solution of SiC in AlN and vice versa were detected, which explains the apparent lack of SiC in the 10-vol.% SiC material. In the high SiC containing materials (>15 vol.% SiC) elongated SiC grains were found on the AlN grain boundaries, as shown in Fig. 5d. These grains were identified as various α-SiC polytypes such as 4H, 5H and 6H.

Vickers hardness, bending strength, Young's modulus and fracture toughness of AlN and the AlN–SiC composites are presented in Fig. 6. The fracture toughness at 800 °C is also included. The Vickers hardness increases strongly with increasing SiC content as is also observed both for solid solution materials [11,24] and particulate composites [3,10,12,27–29]. Adding 30 vol.% SiC gives a 64% increase in Vickers hardness. The hardness of the composites is somewhat higher than calculated by the linear mixing rule using a literature value for pure SiC [3], but comparable to interpolated hardness of particulate AlN–SiC composites reported previously [3,10,12,27–29].

The bending strength of the 10-vol.% SiC material is slightly lower than for pure AlN, but a significant increase (21%) is observed for the 20-vol.% SiC material, giving 359 ± 19 MPa. Compared to interpolated bending

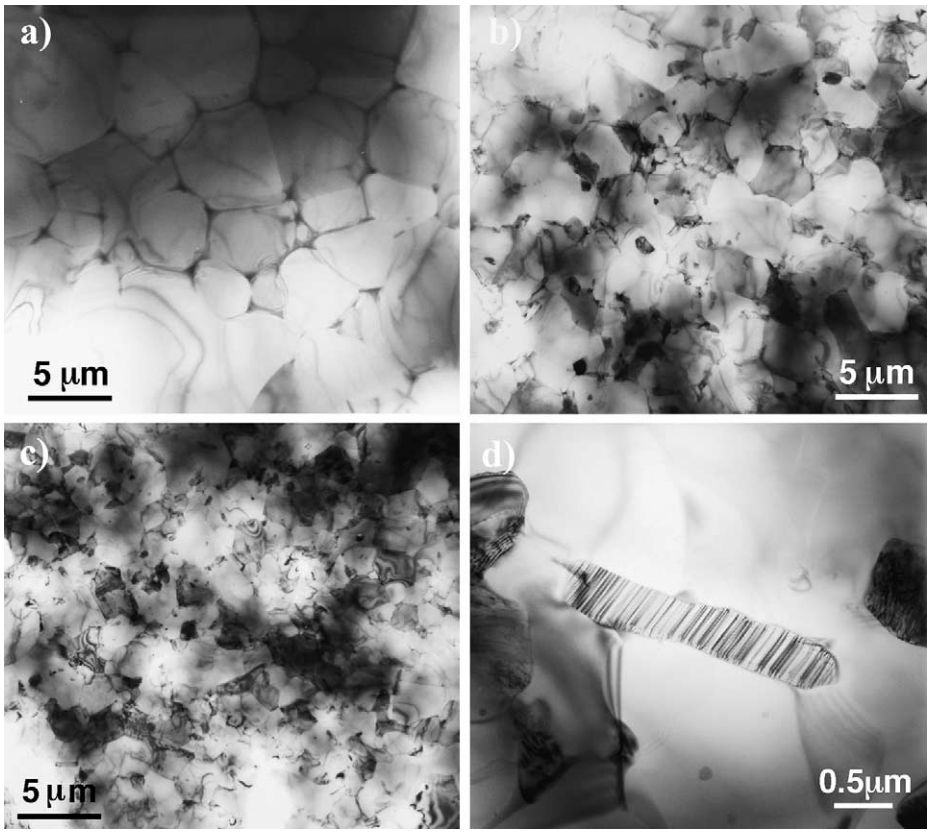

Fig. 5. Low magnification TEM images of AlN–SiC composites. The dark contrast grains are SiC: (a) 10 vol.% SiC, (b) 20 vol.% SiC, (c) 30 vol.% SiC and (d) elongated 5H SiC-grain in the 20-vol.% SiC material.

strength in particulate AlN–SiC composites in the literature [3,5,10,12,21,22] the obtained bending strength is relatively low. The major types of fracture origins for all materials are large (50–100 μm) internal pores or pores located at the surface. Generally, the pores are formed either from volatile contaminations or from inhomogeneous packing of the green body. In the 10-vol.% SiC materials the surface of the pores is covered by yttrium rich phases, caused by agglomeration of the Y_2O_3 during powder mixing. The fracture surfaces from mechanical testing have a larger fraction of intergranular fractures compared to the fracture surfaces formed for SEM analysis (Fig. 3), probably caused by a differing fracture growth.

The Young's modulus is presented together with the Voigt model (upper bounds) and the Reuss model (lower bounds) for Young's modulus of composite materials based on pure AlN and SiC [41,42]. The measured *E*-modulus is considerably higher than the theoretical values and also high compared to the *E*-moduli reported for AlN–SiC solid solution materials [11,25]. A 13% linear increase is observed up to 344 ± 12 GPa for the 20-vol.% SiC material.

The fracture toughness is not significantly changed by addition of 10 vol.% SiC, but a 22% increase up to 4.1 ± 0.2 MPa $m^{1/2}$ is obtained for the 20-vol.% SiC material. The results are in agreement with interpolated values from results presented for particulate AlN–SiC materials [3,5,10,12,27,28]. The fracture toughness of the 20-vol.% SiC material is significantly higher than reported for pure AlN [1–12]. The fracture toughness increases somewhat ($\sim$0.2 MPa $m^{1/2}$) for all the materials from room temperature testing in air to 800 °C and N_2-atmosphere. For pure AlN the fracture mode changes from mainly intergranular at room temperature to mainly transgranular at 800 °C.

The room temperature fracture toughness was also measured by an indentation technique using a Vickers indenter at high load. Different models for calculation of fracture toughness using this method are rearranged to a standard form by Ponton and Rawlings [36] and in Fig. 7 the fracture toughness calculated from selected models are presented together with the measured crack length. The fracture toughness obtained by the SENB method is included for comparison. The different models generally underestimate the fracture toughness compared to the SENB method. For some models, the underestimation is quite large. Most models give a fairly good approximation to the shape of the SENB fracture toughness curve.

4. Discussion

The weight loss during firing is caused by reaction between the AlN or SiC and the oxides (Al_2O_3 and SiO_2)

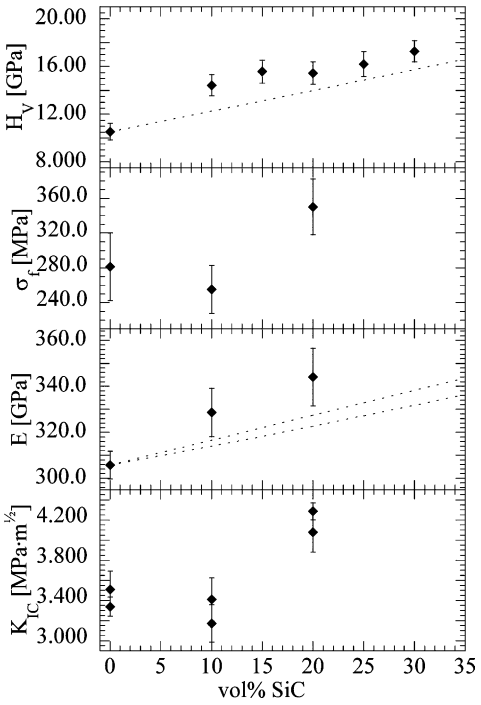

Fig. 6. Vickers hardness, 4-point bending strength, *E*-modulus and fracture toughness (SENB method) of AlN and AlN–SiC composites vs. SiC content. The dotted line in the hardness plot is the linear mixing between Vickers hardness for pure AlN and SiC [3]. The dotted lines in the *E*-modulus plot are the upper (Voigt model) and lower (Reuss model) bounds of the Young's modulus in composite materials calculated from pure AlN and SiC [41,42]. The open diamonds are fracture toughness measured in N_2-atmosphere at 800 °C.

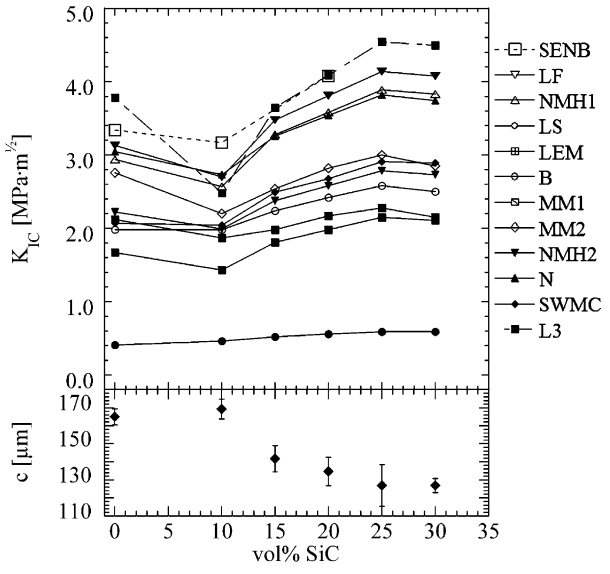

Fig. 7. Fracture toughness (K_{IC}) calculated from crack lengths of Vickers indents versus SiC content, compared with SENB results. The lower part shows the average crack length. The open symbols are models based on a radial-median crack geometry, the filled symbols are models based on a Palmqvist crack geometry. All the calculations are based on the models as presented by Ponton and Rawlings. Also the abbreviations of the different models are obtained from Ponton and Rawlings [36].

found on the powder surface according to reaction (1) and (2) [43].

$$4AlN(s) + Al_2O_3(l) = 3Al_2O(g) + 2N_2(g) \quad (1)$$

$$SiC(s) + 2SiO_2(l) = 3SiO(g) + CO(g) \quad (2)$$

According to Hagen [43], $p_{SiO} > p_{Al_2O}$, which explains the increasing weight loss with increasing SiC content. In the high SiC content materials, >20 vol.% SiC, a considerably increase in weight loss is observed accompanied by a decrease in density. To achieve a high density for high SiC materials (independent of weight loss) higher sintering temperatures or smaller particle size are needed.

Based on the XRD investigations and microstructural studies the solid solution range of SiC in AlN at 1870 °C can be determined. In the material containing 10 vol.% SiC only AlN–SiC solid solution is formed; however, in the 15-vol.% SiC composites, grains of SiC are formed. Above 10 vol.% SiC the lattice parameters also show no change with composition (Fig. 2). Investigations of the AlN–SiC solid solution show that Vegard's law is obeyed in the single-phase area [11,28]. The solubility limit of SiC in AlN is therefore between 10 and 15 vol.% at 1870 °C. The solubility is low compared to the tentative phase diagram presented by Zangvil and Ruh [31]. Both the temperature and composition limits of the solubility range have been discussed by various groups without reaching a definitive agreement [21,26,28,31].

Due to the solid solution of SiC in AlN the 10-vol.% SiC material is not a particulate composite material and is therefore expected to behave similarly to pure AlN rather than the particulate composites. Both Vickers hardness and Young's modulus show a nearly linear increase with increasing SiC content. Both hardness and elastic modulus are dependent on the strength of the atomic bonds and seem not to be dependent on the phase distribution. Bending strength and fracture toughness on the other hand show a small decrease from AlN to 10 vol.% SiC and a large increase from 10 to 20 vol.% SiC. The bending strength of a material is highly dependent on the grain size, the strength decreasing with increasing grain size [44]. In this study the fracture origins are identified as large pores, several times larger than the grain size. It is therefore likely that the bending strength is dependent on the flaw size, not the grain size. The increase in bending strength is also explained by the corresponding increase in fracture toughness for the 20-vol.% SiC material

The fracture mode of pure AlN materials changes from mainly intergranular at room temperature to mainly transgranular at 800 °C without a corresponding decrease in fracture toughness. This fact substantiates the view that crack deflection due to crack growth in preferred atomic planes toughens AlN. Corresponding toughening is also observed in liquid phase sintered AlN–TiN composites [14]. The fracture toughness increases with formation of particulate SiC, even with a decreasing grain size, which demonstrates that the SiC grains are responsible for the observed reinforce-

ment of the AlN–SiC materials. The toughening effect of SiC grains is most likely due to residual strain caused by thermal expansion or elastic modulus mismatch. The presence of elongated SiC grains (Fig. 5d), increases the toughening effect further due to their anisotropy. Elongated SiC grains in AlN–SiC composites were previously only reported for materials containing >50% SiC [10,11,30]. The liquid phase sintering is assumed to be an important factor in the formation of the elongated grains analogous to the elongated plate-like SiC grains which is a requirement for high fracture toughness in in-situ toughened SiC ceramics.

The fracture toughness of both AlN and AlN–SiC materials increased from room temperature to 800 °C. A corresponding effect was observed in AlN–TiN composites when increasing the temperature and the reason was assumed to be the concurrent changing atmosphere from air to N_2. The air has a higher humidity, which might cause corrosion during fracture growth [14]. Mariano et al. [5] reported the fracture toughness to be unchanged between room temperature and 700–800 °C in AlN and 15% SiC-materials, but did not report the atmosphere used.

The different models for calculation of fracture toughness by the use of Vickers indents show a large deviation and underestimate the fracture toughness compared to the SENB method. Somewhat lower values are expected for the indentation technique compared to the SENB method due to smaller flaw size and expected R-curve behaviour [45]. The two models giving the best resemblance to the fracture toughness measured by the SENB method are presented by Lawn and Fuller (LF) [46] and by Niihara (N) [47]. The first model is based on a radial-median crack geometry (penny-like geometry) while the second is based on a Palmqvist crack geometry. Generally, the models based on Palmqvist geometry give higher values than the radial-median crack geometry models. A similar comparative study was performed for AlN–TiN materials [14], also giving a large scattering in fracture toughness and a low resemblance to SENB measurements. The best fit to the SENB values was given by a Palmqvist crack-geometry model presented by Laugier (L3) [48]. From these results it can be concluded that most of the models can be used for comparative studies, but for absolute fracture toughness values the results must be used with great care and identification of the model is important.

5. Conclusions

Dense and homogenous AlN–SiC materials were obtained by pressureless sintering. The density decreased abruptly for materials with more than 20 vol.% SiC. The solubility limit of SiC in AlN at 1870 °C was determined to be between 10 and 15 vol.%. Above 10 vol.% SiC, particulate composites were formed and the SiC grains inhibited AlN grain growth during sintering. Vickers hardness and Young's modulus increased monotonically when adding SiC, 30 vol.% SiC gave a 65% increase in Vickers hardness and 20 vol.% SiC gave a 13% increase in *E*-modulus. Both bending strength and fracture toughness showed a slight decrease when a 10 vol.% SiC solid solution was formed, but a total addition of 20 vol.% SiC gave 21 and 22% increase, respectively, compared to pure AlN. The toughening of the composites was due to residual strain due to thermal expansion or elastic modulus mismatch between SiC grains and the AlN–SiC matrix. Elongated α-SiC grains were observed for >15-vol.% SiC materials and increased the toughening effect of the materials.

Acknowledgements

The Research Council of Norway is acknowledged for financial support.

References

[1] S.R. Witek, G.A. Miller, M.P. Harmer, Effects of CaO on the strength and toughness of AlN, J. Am. Ceram. Soc. 72 (3) (1987) 469–473.
[2] R.F. Cook, B.R. Lawn, C.J. Fairbanks, Microstructure–strength properties in ceramics. I. Effect of crack size on toughness, J. Am. Ceram. Soc. 68 (1985) 604–615.
[3] J.-L. Huang, J.-M. Jih, Investigation of SiC–AlN. Part II. Mechanical properties, J. Am. Ceram. Soc. 79 (5) (1996) 1262–1264.
[4] E. Hagen, Y.D. Yu, T. Grande, R. Høier, M.-A. Einarsrud, Sintering of AlN ceramics using $CaO–Al_2O_3$ as sintering additive chemistry and microstructural development, J. Am. Ceram. Soc. 85 (12) (2002) 2971–2976.
[5] S.A. Mariano, D. Friel, I. Bar-On, Elevated temperature mechanical properties of SiC–AlN particulate composites, Ceram. Eng. Proc. 14 (1993) 1077–1088.
[6] H. Hunold, Herstellung, Eigenschaften und Anwendungsmöglichkeiten von Aluminiumnitrid-Bauteilen, Metall 3 (1990) 266–269.
[7] J. Tatami, K. Komeya, T. Meguro, S. Iwasawa, R. Terao, Fracture behaviour of strengthened AlN, Ceram. Trans. 106 (2000) 494–499.
[8] M. Tajika, H. Matsubara, W. Rafaniello, Microstructures and properties in aluminium nitride–titanium nitride composite ceramics, Mater. Lett. 41 (1999) 139–144.
[9] M. Tajika, H. Matsubara, W. Rafaniello, J. Hojo, Development of synergistic AlN ceramics by simultaneous addition of BN and TiN, J. Mater. Sci. Lett. 20 (2001) 201–203.
[10] J.-F. Li, R. Watanabe, Pressureless sintering and high-temperature strength of SiC–AlN ceramics, J. Ceram. Soc. Jpn. 102 (8) (1994) 727–731.
[11] H. Lubis, N.L. Hecht, G.A. Graves Jr., R. Ruh, Microstructure–property relations of hot-pressed silicon carbide–aluminum nitride compositions at room and elevated temperatures, J. Am. Ceram. Soc. 82 (9) (1999) 2481–2489.
[12] Y. Kobayashi, J.-F. Li, A. Kawasaki, R. Watanabe, Microstructure and high-temperature property of reaction HIP-sintered SiC–AlN ceramic alloys, Mater. T. JIM 37 (4) (1996) 807–812.
[13] R. Terao, J. Tatami, T. Meguro, K. Komeya, Fracture behaviour of AlN ceramics with rare earth oxides, J. Eur. Ceram. Soc. 22 (2002) 1051–1059.
[14] I.-L. Tangen, Y.D. Yu, T. Grande, R. Høier, M.-A. Einarsrud, Preparation and characterisation of aluminium nitride–titanium nitride composites, J. Eur. Ceram. Soc. 24 (2004) 2169–2179.

[15] Y.G. Tkachenko, D.Z. Yirchenko, G.S. Oleinik, O.A. Shevchenko, S.A. Satanin, Self-reinforced materials based on aluminium nitride, Sov. Powder Metall. 31 (1992) 785–789.
[16] M.A. Kuzenkova, P.S. Kislyi, O.V. Pshenichaya, Structure and properties of composites based on Ti, Inorg. Mater. 12 (1976) 371–374.
[17] S. Nakahata, T. Matsuura, K. Sogabe, A. Yamakawa, Analysis of Ti compound particle distribution in AlN-matrix composites, Ceram. Trans. 44 (1994) 221–231 (The American Ceramic Society).
[18] M. Tajika, H. Matsubara, W. Rafaniello, Microstructural development in AlN composite ceramics, Nanostruct. Mater. 12 (1999) 131–134.
[19] K.S. Mazdiuasni, R. Ruh, E.E. Hermes, Phase characterization and properties of AlN–BN composites, Am. Ceram. Soc. Bull. 64 (8) (1985) 1149–1154.
[20] Y. Xu, A. Zangvil, M. Landon, F. Thevenot, Microstructure and mechanical properties of hot-pressed silicon carbide–aluminum nitride compositions, J. Am. Ceram. Soc. 75 (2) (1992) 325–333.
[21] J.-F. Li, A. Kawasaki, R. Watanabe, High temperature strength of SiC–AlN solid solutions and composites as evaluated by small punch tests, J. Jpn. Inst. Metals. 56 (12) (1992) 1450–1456.
[22] H.A. Toutanji, D. Friel, T. El-Korchi, R.N. Katz, G. Wechsler, W. Rafaniello, Room temperature tensile and flexural strength of ceramics in AlN–SiC system, J. Eur. Ceram. Soc. 15 (1995) 425–434.
[23] J.-L. Huang, J.-M. Jih, Investigation of SiC–AlN. Part I. Microstructure and solid solution, J. Mater. Res. 10 (1995) 651–658.
[24] R. Ruh, A. Zangvil, Composition and properties of hot-pressed SiC–AlN solid solutions, J. Am. Ceram. Soc. 65 (5) (1982) 260–265.
[25] G.K. Safraliev, Yu.M. Tairov, V.F. Tsvetkov, Sh.Sh. Shabanov, E.G. Pashchuk, N.V. Ofitserova, D.D. Avrov, S.A. Sadykov, Preparation and properties of polycrystalline SiC–AlN solid solutions, Semiconductors 27 (3) (1993) 224–227.
[26] M. Landon, F. Thevenot, The SiC–AlN system: influence of elaboration routes on the solid solution formation and its mechanical properties, Ceram. Int. 17 (1991) 97–110.
[27] V.A. Melnikova, V.K. Kazakov, A.N. Pilyankevich, Structure of ceramics of the AlN–SiC system, Sov. Powder. Metall 27 (1988) 498–502.
[28] R.-R. Lee, W.-C. Wei, Fabrication, microstructure, and properties of SiC–AlN ceramic alloys, Ceram. Eng. Sci. Proc. 11 (7/8) (1990) 1094–1121.
[29] M. Miura, T. Yogo, S.-I. Hirano, Phase separation and toughening of SiC–AlN solid-solution ceramics, J. Mater. Sci. 27 (1993) 3859–3865.
[30] W. Choi, H. Kim, J.-K. Lee, Grain morphology of SiC–AlN ceramics prepared by pressureless sintering, J. Mater. Sci. Lett. 14 (1995) 1585–1586.
[31] A. Zangvil, R. Ruh, Phase relationships in the SiC–AlN system, J. Am. Ceram. Soc. 71 (10) (1988) 884–890.
[32] O. Herstad, K. Motzfeldt, Vapour pressures in the system Al–Al_2O_3. The effusion method and pressure compensation methods, Rev. Hautes Temper. Et Réfract. 3 (1966) 291–300.
[33] F. Sass, C. Bouché, A. Leitner, Dubbels Taschenbuch für den Maschinenbau, Springer-Verlag, Berlin, 1961.
[34] ISO/CD 15732 Fine Ceramics (Advanced Ceramics, Advanced Technical Ceramics)—Test Method for Fracture Toughness at Room Temperature by Single Edge Precracked Beam (Sepb) Method, International Organization for Standardization, Geneva, Switzerland.
[35] G.R. Anstis, P. Chantikul, B.R. Lawn, D.B. Marshall, A critical evaluation of indentation techniques for measuring fracture toughness. I. Direct crack measurements, J. Am. Ceram. Soc. 64 (1981) 533–538.
[36] B. Ponton, R.D. Rawlings, Vickers indentation fracture toughness test. Part I. Review of literature and formulation of standardised indentation toughness equations, Mater. Sci. Technol. 5 (1989) 865–872.
[37] J. Gröbner, H.L. Lukas, F. Aldinger, Thermodynamic calculations of the quasibinary Al_2O_3–Y_2O_3 system and the Y–Al–O ternary system, Z. Metallkd. 87 (1996) 268–273.
[38] W.Y. Sun, Z.K. Huang, T.Y. Tien, T.S. Yen, Phase relationships in the system Y–Al–O–N, Mater. Lett. 11 (1991) 67–69.
[39] J.A. Kohn, P.G. Cotter, R.A. Cotter, Synthesis of aluminum nitride monocrystals, Am. Mineral. 41 (3/4) (1956) 355–358 (PDF 25-1133).
[40] J. Bind, Private communication, Penn State University, USA (PDF 29-1126), 1977.
[41] W.D. Kingery, H.K. Bowen, D.R. Uhlmann, Introduction to Ceramics, John Wiley & Sons, New York, 1976.
[42] D.W. Richerson, Modern Ceramic Engineering, Marcel Dekker, Inc., New York, 1992.
[43] E. Hagen, AlN and AlN/SiC Ceramic Sidelining Materials in Aluminium Electrolysis Cells, Dr. ing Thesis, Norwegian University of Science and Technology, Trondheim, 2000.
[44] P. Knudsen, Dependence of mechanical strength of brittle polycrystalline specimens on porosity and grain size, J. Am. Ceram. Soc. 42 (1959) 376–387.
[45] D.C. Cranmer, D.W. Richerson, Mechanical Testing Methodology for Ceramic Design and Reliability, Marcel Dekker, Inc., New York, 1998.
[46] B.R. Lawn, E.R. Fuller, Equilibrium penny-like cracks in indentation fracture, J. Mater. Sci. 10 (1975) 2016–2024.
[47] K. Niihara, A fracture mechanics analysis of indentation-induced palmqvist crack in ceramics, J. Mater. Sci. Lett. 2 (1983) 221–223.
[48] M.T. Laugier, New formula for indentation toughness in ceramics, J. Mater. Sci. Lett. 6 (1987) 355–356.